

# Select2Drive: Pragmatic Communications for Real-Time Collaborative Autonomous Driving

Jiahao Huang, Jianhang Zhu, Rongpeng Li, Zhifeng Zhao, and Honggang Zhang

**Abstract**—Vehicle-to-Everything communications-assisted Autonomous Driving (V2X-AD) has witnessed remarkable advancements in recent years, with pragmatic communications (PragComm) emerging as a promising paradigm for real-time collaboration among vehicles and other agents. Simultaneously, extensive research has explored the interplay between collaborative perception and decision-making in end-to-end driving frameworks. In this work, we revisit the collaborative driving problem and propose the Select2Drive framework to optimize the utilization of limited computational and communication resources. Particularly, to mitigate cumulative latency in perception and decision-making, Select2Drive introduces Distributed Predictive Perception (DPP) by formulating an active prediction paradigm and simplifies high-dimensional semantic feature prediction into computation cost-efficient, motion-aware reconstruction. Given the “less is more” principle that a broadened perceptual horizon possibly confuses the decision module rather than contributing to it, Select2Drive utilizes Area-of-Importance-based PragComm (APC) to prioritize the communications of critical regions, thus boosting both communication efficiency and decision-making efficacy. Empirical evaluations on the V2Xverse dataset [1] and CARLA driving simulator [2] demonstrate that Select2Drive achieves a 11.31% (resp. 7.69%) improvement in offline perception tasks under limited bandwidth (resp. pose error conditions). Moreover, it delivers at most 14.68% and 31.76% enhancement in closed-loop driving scores and route completion rates, particularly in scenarios characterized by dense traffic and high-speed dynamics.

**Index Terms**—Collaborative perception, End-to-end driving, V2X-Communications, Pragmatic communications

## I. INTRODUCTION

Due to the inherent limitations of Autonomous Driving (AD), such as restricted visibility, unpredictability of other road users [3]–[6], and difficulties in determining optimal paths [7], Vehicle-to-Everything (V2X) Communications becomes an indispensable ingredient in the Internet of Vehicles. By enabling the exchange of complementary information among vehicles, roadside units (RSUs), and even pedestrians [8], V2X communications promise a broadened perceptual horizon for individual autonomous vehicles, contributing to timely identifying emergent objects beyond visual observations [9] and swiftly making proper responses [10]. Conventionally, early studies in the field of V2X communications focus on the realization of ubiquitous connectivity [11], [12] for accomplishing collaborative perception [9]. However, the

J. Huang, J. Zhu, and R. Li are with Zhejiang University, Hangzhou 310027, China, (email: {22331083, zhujh20, lirongpeng}@zju.edu.cn).

Z. Zhao is with Zhejiang Lab, Hangzhou 310012, China, as well as Zhejiang University, Hangzhou 310027, China (email: zhaozf@zhejianglab.com).

H. Zhang is with City University of Macau, Macau, China (email: hgzhang@cityu.edu.mo).

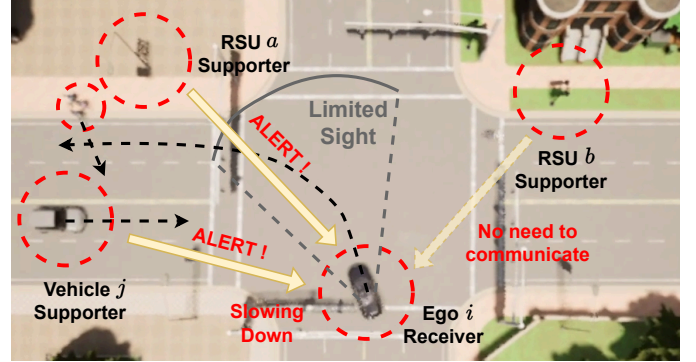


Fig. 1: Overview of V2X-AD. Contingent on pragmatic communications of driving-critical information with nearby supporters (e.g., vehicles and RSUs), the Ego vehicle maintains safe AD.

associated communication costs scale linearly with the size of the perceptual region [13] and the time duration grows quadratically with the number of collaborating agents, placing significant demands on even next-generation 6G communication systems [14]. Meanwhile, collaborative perception within a small number of neighboring agents and a limited timeframe only yields marginal performance improvement over single-agent perception [15]. Fortunately, for V2X communications-assisted AD (V2X-AD), its sole involvement of reliable communications and the ignorance over the lasting impact of perception results on autonomous driving decisions still leave enormous optimization room. In other words, the Pragmatic Communications (PragComm)<sup>1</sup>, which aims to deliver compact latent representations tailored to specific downstream decision-making tasks [20], can better take account of both collaborative perception according to sensor data and subsequent driving decision simultaneously [21]. In the context of V2X-AD, the PragComm is commonly deployed as a compression paradigm [15]–[17], [19], [22]. These methods operate under a fundamental assumption: during each time interval  $\tau$ , all participating agents first broadcast Basic Safety Messages (BSMs) and subsequently decide whether to engage in communication [16] or exchange valuable perception blocks [15]. However, this approach presumes an idealized scenario in which the entire process, regardless of the number of point-to-point communication links, can be completed within each  $\tau$ . Apparently, this assumption is impractical due to inevitable

<sup>1</sup>It is also known as pragmatic compression or effective communications in the literature.

TABLE I: A comparison between Select2Drive and related works.

References	Realistic Communications	Latency Considered	Perception Involved	Driving-Task Oriented	Brief Description
[1]	○	○	●	●	Integrates basic collaborative perception into closed-loop driving, lacks communication frameworks and real-world latency simulation.
[10]	●	○	○	●	A blind-spot warning mechanism without engaging in precise collaborative perception and lack of generalization ability.
[16], [17]	○	○	●	○	Fetches the most valuable information for exchange under the premise of an ideal communication assumption, susceptible to latency issues.
[18], [19]	○	●	●	○	A centralized estimation upon the timing of incoming information, imposes significant challenges on mobile devices' computational and storage capacities.
[13]	●	●	●	○	A centralized, latency-based collaborator selection mechanism, incorporating the receiver's historical data into perception, proves inefficient in utilizing communication resources effectively.
Ours	●	●	●	●	Implementation of a distributed prediction mechanism to mitigate overall latency, and pre-filtering invaluable information based on driving context before communication.

Notations: ○ indicates not included; ● indicates fully included.

latency from transmission and inference delays<sup>2</sup>.

On the other hand, despite advancement in collaborative perception, a critical gap lies in understanding how perception enhancements impact integrated, system-level driving performance. Typically, Imitation Learning (IL) [4], [5], [23], [24] instead of Reinforcement Learning (RL) [3] is adopted owing to the remarkable performance of Behavior Cloning (BC) in scenarios with predefined routes. Counterintuitively, as shown in findings from Ref. [4], [5], particularly under augmented, collaborative perception, an expanded field of vision does not consistently improve driving outcomes, advocating for a “*less is more*” principle in V2X-AD. In other words, for closed-loop driving tasks, isolated perception modules often fail to seamlessly benefit subsequent planning and control stages, while incurring troublesome *error propagation*, since inaccuracies in perception accumulate through the system [7]. Therefore, in order to address latency-induced collaborative perception inconsistencies and ensure a consistent driving improvement, PragComm shall be re-developed beyond simple context compression.

In this paper, we propose Select2Drive, a revamped PragComm-based framework that not only accounts for the compensation of overall latency but also incorporates calibrations tailored for eliminating error propagation in V2X-AD. Particularly, on top of a formulated delivery model that contributes to evaluating the underlying physical transmission plausibility [25], [26], Select2Drive introduces a novel Distributed Predictive Perception (DPP) module, which capably predicts future semantic features using low-level indicators. Notably, despite the conceptual simplicity, implementing DPP is non-trivial as the limited computational capability requires precise forecasting of future states from high-dimensional voxel flow or pseudo-maps [27], focusing on minimizing disparities between predicted and current heatmaps. Furthermore, inspired by the underscored benefits of constrained observational horizons [28], [29], Select2Drive investigates the feasibility of decision-making strategies using minimal observation content. This finally culminates in an Area-of-

Importance-based PragComm (APC) framework, which prioritizes communications in driving-critical regions. While providing key distinctions with highly relevant literature in Table I, our key contribution could be summarized as follows:

- To significantly boost the closed-loop driving performance under the impact of communication and computational latency, we propose a PragComm-based, IL-enabled real-time collaborative driving framework Select2Drive. Beyond simple information compression, the DPP and APC components therein can effectively incorporate background vehicle information while avoiding redundant computational burden and minimizing unnecessary communications.
- The calibrated DPP component integrates a predictive mechanism and a motion-aware affine transformation, which leverages low-dimensional motion flow to infer future semantic features. Avoiding direct prediction of high-dimensional BEV semantic features [18] effectively mitigates timeliness challenges without introducing significant computational cost.
- Bearing the “*less is more*” principle in mind, we introduce a revamped APC component that restricts the communication region to the Area-of-Importance (AoIm), effectively alleviating the *covariate shift* [30] induced by BC on constrained datasets. Therefore, Select2Drive enables prioritized communications in driving-critical regions and solves the latency-induced fusion inconsistencies from collaborative perception.
- Building upon the CARLA Simulator [2] and prior studies [1], we develop a comprehensive simulation platform<sup>3</sup> that transitions collaborative perception approaches [13], [16], [17] from offline datasets to closed-loop driving scenarios [31] while offering an extensible interface for multi-vehicle cooperative driving. Through extensive experiments on both collaborative perception tasks and online closed-loop driving tasks, we demonstrate significantly improved performance (e.g., 11.31% higher perception accuracy, 14.68% higher closed-loop driving

<sup>2</sup>Latency here specifically refers to the minimum response time required for a background vehicle to collect, process, and transmit data until the information fused at the ego vehicle.

<sup>3</sup>The open-source codes can be found at <https://github.com/zjunice> once the manuscript has been accepted.

scores, and 31.76% larger route completion rates) of Select2Drive across diversified communications-limited scenarios.

The remainder of this paper is organized as follows. We introduce related works in Section II. We introduce system models and formulate the problem in Section III. In Section IV, we elaborate on the details of our proposed prediction paradigm. In Section V, we present the experimental results and discussions. Finally, Section VI concludes this paper.

## II. RELATED WORKS

### A. End-to-end Autonomous Driving

Recent advancement [4], [5] in learning-based end-to-end autonomous driving, which directly translates environmental observations into control signals and conceptually addresses the cascading errors of traditional modular design, has positioned this domain as a pivotal research focus. Nevertheless, existing methods [13], [16], [17] highlight a gap between theoretical assumption and practical implementation. For example, Ref. [9] demonstrates the performance of collaborative perception algorithms in simulated environments but rarely applies them to real-world driving tasks. Ref. [32] assumes accurate agent position data, which is often impractical in real-world scenarios. Our approach bridges this gap by integrating theoretical strategies with higher-fidelity implementations, which utilize perception data directly from emulated raw sensor inputs for more realistic analysis.

**Learning Approaches:** End-to-end driving approaches can be classified into RL-based [3] or supervised learning-based IL [23]<sup>4</sup>. Compared to RL-based solutions, IL progressively benefits from the increasing perception performance, leading to a stable enhancement in the learning of driving tasks through BC [4], [5]. Notably, BC demonstrates effective performance for in-distribution states within the training dataset but struggles to generalize to out-of-distribution (OOD) states due to compounding action errors, a phenomenon termed *covariate shift* [30]. To mitigate this, we intentionally add noise to ensure more states within the training distribution [33].

**AD:** Ref. [10] proposes a visually cooperative driving framework that aggregates voxel representations from multiple collaborators to improve decision-making. Ref. [6] demonstrates that besides challenges in predicting the motion of out-of-view or non-interactive objects, single-agent driving systems inherently struggle with occluded or distant regions, often leading to catastrophic failures. To address these limitations, V2X-AD adopts a multi-agent collaborative paradigm leveraging V2X communications, enabling vehicles to share information and collaboratively inform decisions [17]. Despite the remarkable progress, the latest evaluation platform [1] remains constrained by idealized communication assumptions.

<sup>4</sup>Traditional RL/IL methods are typically limited to lower-dimensional problems. Therefore, the methodologies discussed in this paper specifically refer to Deep Learning (DL)-driven RL/IL approaches.

### B. Pragmatic Communications

Commonly formulated as an extension of the Markov Decision Process (MDP) framework [28], PragComm [34] shifts the focus from accurate bit transmission or precise semantic interpretation to capturing key information and creating compact representations for specific downstream tasks.

**V2X Communications:** PragComm is contingent on the underlying capability of V2X communications [8], such as IEEE 802.11p-based DSRC [35] and the 3GPP Cellular-based V2X (C-V2X) [36]. Both architectures define BSMs [37], [38], transmitted periodically at up to 10 Hz to convey critical state information such as position, dynamics, and vehicle status. Correspondingly, high-frequency BSMs can serve as a foundation for high-dimensional semantic feature communications, minimizing redundant transmissions. For DSRC-based transmission, bandwidth-limited channel conditions highlight the necessity to investigate the impact of communication latency on collaborative perception, while the reliance on inter-node routing in C-V2X-based transmission necessitates a focus on systemic overall delays.

**PragComm in V2X-AD:** Ref. [17] establishes a PragComm-based framework towards achieving a balance between perception performance and communication costs in V2X-AD. It employs a two-step strategy: (1) semantic feature extraction from raw sensory data to low-level heatmaps as indicators; (2) selective transmission of high-value semantic features for fusion to optimize communication efficiency. However, considering the heterogeneity in distance and content [22], PragComm in V2X-AD encounters difficulties spanning from localization uncertainty [19] to clock synchronization and dynamic delay compensation [18]. For example, even minimal delays can profoundly undermine the timeliness of transmitted information, potentially incurring catastrophic outcomes [8]. Meanwhile, prior methodologies primarily focus on reconstructing the distribution of proximal objects. While enhancing perception, these methods often misalign with driving policy optimization, necessitating integrated frameworks for cohesive performance. In that regard, Ref. [28] underscores that the decoupling of learning and communications yields suboptimal results. Therefore, there emerges a strong incentive to revamp PragComm for AD.

Compared to the literature, Select2Drive employs DPP, which diverges from traditional approaches by integrating a prediction mechanism at the supporter level to proactively mitigate transmission latency, to alleviate the impact of inevitable delays without imposing considerable burdens on computations. Meanwhile, Select2Drive takes advantage of APC to bridge the disconnection between perception modules and low-level controllers by explicitly incorporating prior trajectory information into communication strategies. Therefore, Select2Drive not only further minimizes communication overhead but also sharpens the model's focus on task-critical information, ultimately enhancing driving performance.

## III. SYSTEM MODEL AND PROBLEM FORMULATION

Beforehand, primary notations used in this paper are summarized in Table II. In the subsequent discourse, intermediate

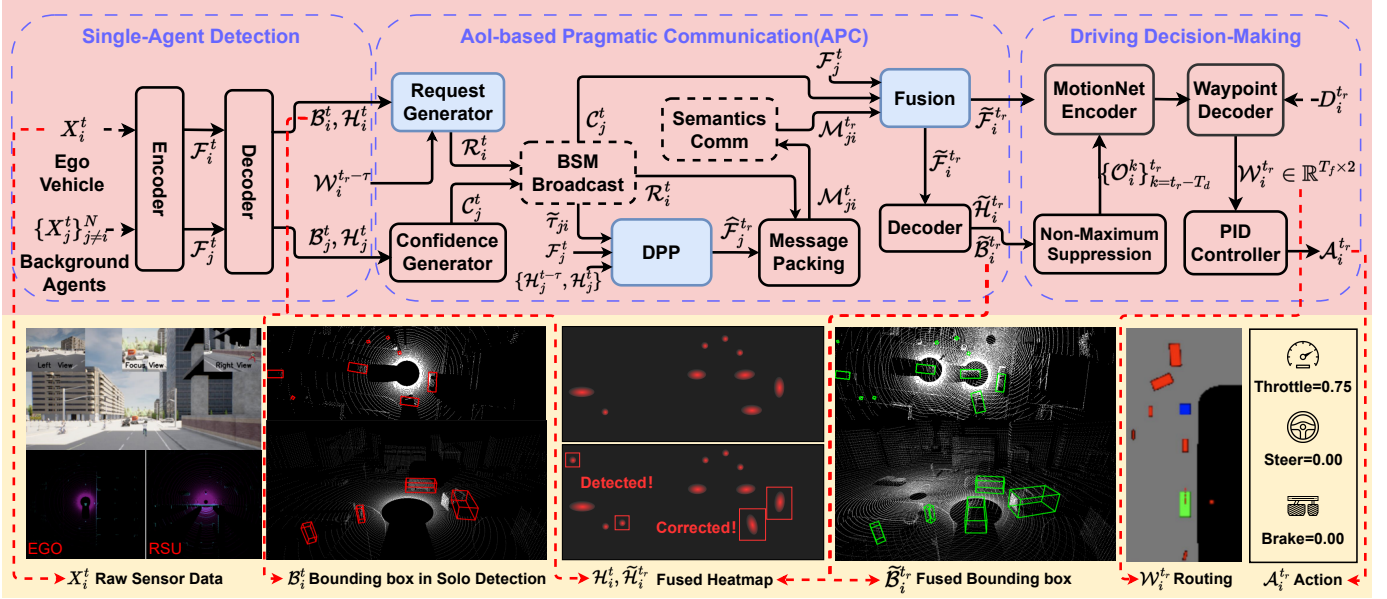


Fig. 2: System model of our V2X-AD framework encompassing perception, decision-making, and control stages. The upper section provides a detailed closed-loop flowchart, illustrating the iterative cycle from perception to action, while incorporating feedback into subsequent iterations. The lower section visually depicts the complete decision-making process, emphasizing the sequential flow of actions and data exchange.

TABLE II: A summary of major notations used in this paper.

Notation	Definition
$X_i^t, \mathcal{F}_i^t$	Raw sensor data and Latest available semantic Features of agent $i$ at time $t$
$\mathcal{H}_i^t, \mathcal{B}_i^t$	Heatmap and Bounding box in the view
$\mathcal{H}_j^{t-\tau}, \mathcal{H}_j^t$	Historical heatmaps
$\hat{\mathcal{H}}_j^{tr}, \hat{\mathcal{F}}_j^{tr}$	Forecasted heatmap and processed semantic features
$C_j^t, \mathcal{R}_i^t$	Confidence Map of Agent $j$ and Request Map of agent $i$
$\tilde{\mathcal{F}}_i^{tr}, \tilde{\mathcal{H}}_i^{tr}, \tilde{\mathcal{B}}_i^{tr}$	Fused semantic feature and collaborated perception
$\{\mathcal{O}_i^k\}_{k=t_r-T_d}^{t_r}$	$T_d$ frames of historical BEV occupancy maps
$\tilde{\mathcal{F}}_i^{tr}, \tilde{\mathcal{H}}_i^{tr}, \tilde{\mathcal{B}}_i^{tr}$	Fused semantic feature and collaborated perception
$\mathcal{W}_i^{tr}, \mathcal{A}_i^{tr}$	Driving trajectory and driving action
$\Delta\tau$	Broadcast period
$\delta\tau_{ji}, \tilde{\delta}\tau_{ji}$	Overall transmission latency and estimated one between agent $j$ and agent $i$
$\tau_{ji}, \tilde{\tau}_{ji}$	Real systematic latency and estimated one between agent $j$ and agent $i$

variables output by the Deep Neural Network (DNN) will be denoted using a script font (e.g.,  $\mathcal{F}_i^t$ ), while directly observable variables will be represented in a standard font (e.g.,  $D_i^{tr}$ ). In addition, a DNN will be denoted as a function  $\Phi(\cdot)$ .

### A. System Model

In this paper, we consider a collaborative perception-based AD scenario with multiple vehicles (i.e., agents). Particularly,

as shown in Fig. 2, let  $t$  represent the moment when an agent  $i$  initiates a decision-making cycle. At time  $t$ , agent  $i$  can perceive raw data (e.g., RGB images and 3D point clouds) at a fixed interval  $\tau$ , while the communications possibly occur between any ego agent  $i$  and one of its supporting neighbors  $j$  (i.e., background vehicles and RSUs). Afterwards, agent  $i$  aims to maximize the accomplishment rate of its IL-based driving task with driving plan  $\mathcal{W}_i^{tr}$ , contingent on the fusion of its own observed raw data  $X_i^t$  and exchanged information  $\{\mathcal{M}_{j_i}^t\}_{\mathcal{N}_i^t}$  from neighboring agents  $j \in \mathcal{N}_i^t$ . Basically, such a scenario can be classified as a pragmatic communications-based MDP.

1) *Confidence-Driven Message Packing* After obtaining the raw sensor data  $X_i^t$ , each vehicle leverages an encoder  $\Phi_{\text{encoder}}$ , which consists of a series of 2D convolutions and max-pooling layers, to yield the latest available semantic features  $\mathcal{F}_i^t$  that merges RGB images and 3D point clouds into a unified global coordinate system, namely

$$\mathcal{F}_i^t = \Phi_{\text{encoder}}(X_i^t) \in \mathbb{R}^{H \times W \times D}, \quad (1)$$

where  $H$ ,  $W$ , and  $D$  denote the dimensions of the pseudo-image. Typically,  $D \gg 1$  even only 3D point clouds are utilized. Subsequently, a decoder  $\Phi_{\text{decoder}}$ , composed of several deconvolution layers [39], is employed to generate a probability heatmap  $\mathcal{H}_i^t$  and a bounding box regression map  $\mathcal{B}_i^t$ . The heatmap  $\mathcal{H}_i^t$  represents the spatial likelihood of an object (e.g., vehicles, pedestrians, or traffic signs) being present in an image or frame, while the regression map  $\mathcal{B}_i^t$  provides precise localization details (e.g., center coordinates, width, and height) for detected objects, respectively. Therefore,

$$\mathcal{H}_i^t, \mathcal{B}_i^t = \Phi_{\text{decoder}}(\mathcal{F}_i^t) \in \mathbb{R}^{H \times W \times C}, \mathbb{R}^{H \times W \times 8C}, \quad (2)$$

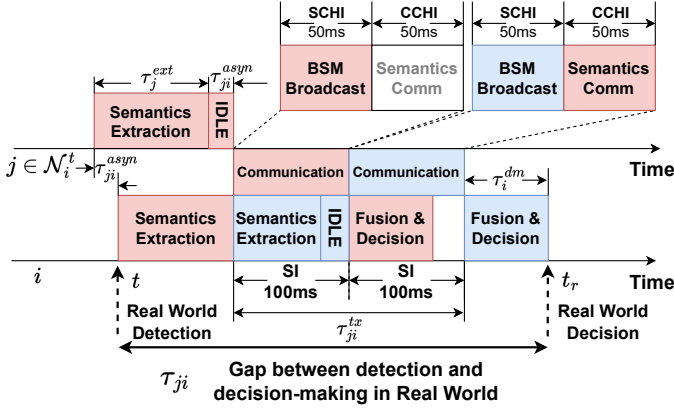


Fig. 3: Flow chart from the perspective of agent  $i$ . The red box delineates the decision cycle initiated at time  $t$ , while the blue box represents the subsequent cycle commencing at time  $t + \tau$ . The interval between consecutive perception and communication phases is uniformly set to  $\tau$ .

with  $C$  representing the number of object categories and  $C = 3$  if three categories, i.e. vehicles, bicycles, and pedestrians, are detected.

Afterward, consistent with [17], the agent  $i$  sends low-dimensional BSMs, including an  $\Phi_{\text{Gen}}$ -induced confidence map  $\mathcal{C}_i^t$  and a request map  $\mathcal{R}_i^t$ , as

$$\mathcal{C}_i^t = \Phi_{\text{Gen}}(\mathcal{H}_i^t) \in [0, 1]^{H \times W}, \quad (3)$$

$$\mathcal{R}_i^t = 1 - \mathcal{C}_i^t \in [0, 1]^{H \times W}, \quad (4)$$

where  $\Phi_{\text{Gen}}$  denotes a maximum operation in the third dimension followed by a Gaussian filter. Under the ideal latency-free assumption, for the supporting vehicle  $j \in \mathcal{N}_i^t$ , confidence-driven messages for feedback are given as

$$\mathcal{M}_{ji}^t = \mathcal{F}_j^t \times \mathcal{P}_{ji}^t \in \mathbb{R}^{H \times W \times D}. \quad (5)$$

Here,  $\mathcal{P}_{ji}^t = \mathbf{1}(\mathcal{R}_i^t \odot \mathcal{C}_j^t \geq p_{\text{thre}}) \in \mathbb{R}^{H \times W}$  indicates a spatial selection mechanism for  $\mathcal{F}_j^t$ , and  $p_{\text{thre}}$  is a hyperparameter controlling the extent of collaboration. The indicator  $\mathbf{1}(\cdot)$  equals 1 if the condition is met; while nulls otherwise. The operator  $\odot$  denotes element-wise multiplication.

2) *Latency Model* The acquirement, communications and post-processing of  $\mathcal{M}_{ji}^t$  inevitably incur some latency, such as the computational latency involved in semantic extraction  $\tau_j^{\text{ext}}$  and post-processing for decision-making  $\tau_i^{\text{dm}}$ , the asynchronous inter-agent timing differences  $\tau_{ji}^{\text{asyn}}$ , and the more prominently communication latency<sup>5</sup>  $\tau_{ji}^{\text{tx}}$ .

As depicted in Fig. 3, to quantify  $\tau_{ji}^{\text{tx}}$ , a verification mechanism proposed in [25], [26] is employed. Notably, in the multi-channel alternating switch mode therein, the communication process is structured into a Synchronization Interval (SI), denoted as  $\tau$ , which is further divided into a Service Channel Interval (SCHI) and a Control Channel Interval (CCHI), each lasting  $\Delta\tau$ . During the SCHI, BSMs like  $(\mathcal{R}_i^t$  and  $\mathcal{C}_i^t)$  are

broadcast, while semantic information  $\mathcal{M}_{ji}^t$  is transmitted during the subsequent CCHI. The minimum transmission time for  $\mathcal{M}_{ji}^t$  is given by

$$\tau_{ji}^{\text{tx}} = \tau_{ji}^{\text{pr}} + \tau_{ji}^{\text{net}}. \quad (6)$$

Here,  $\tau_{ji}^{\text{pr}}$  represents the propagation latency, computed as per 3GPP TR 38.901 [40], that is,  $\tau_{ji}^{\text{pr}} = \text{size}(\mathcal{M}_{ji}^t) / (b_{ji} \log_2(1 + 10^{0.1(p_{ji}^{\text{tx}} - p_{ji}^{\text{loss}} - p_{ji}^{\text{noise}})}))$ , where  $b_{ji}$  is the bandwidth allocated per agent,  $p_{ji}^{\text{tx}}$  is the transmission power,  $p_{ji}^{\text{noise}}$  is the noise power, and  $p_{ji}^{\text{loss}}$  denotes the path loss calculated by  $p_{ji}^{\text{loss}} = 28 + 22 \log_{10}(d_{ji}) + 20 \log_{10}(f_c)$  [40], with  $d_{ji}$  being the inter-agent distance (in meters) and  $f_c$  the carrier frequency (in GHz). The term  $\tau_{ji}^{\text{net}}$  accounts for the processing time at network nodes (e.g., routers, switches, base stations) before forwarding data to the next hop. Owing to the direct communication characteristics of DSRC-based transmission,  $\tau_{ji}^{\text{tx}}$  is predominantly constrained by  $\tau_{ji}^{\text{pr}}$ , with negligible  $\tau_{ji}^{\text{net}}$  [8]. Conversely, the multicast service in C-V2X-based transmission effectively mitigates  $\tau_{ji}^{\text{pr}}$  while introducing substantial  $\tau_{ji}^{\text{net}}$  delays, primarily attributed to computational burdens at network nodes caused by access and handover overhead [41].

In a nutshell, the overall latency  $\tau_{ji}$  can be expressed as:

$$\tau_{ji} = \tau_j^{\text{ext}} + \tau_{ji}^{\text{asyn}} + \tau_{ji}^{\text{tx}} + \tau_i^{\text{dm}}. \quad (7)$$

For notational simplicity,  $t_r$  denotes the moment when the  $i$  obtains the message  $\mathcal{M}_{ji}^t$  from another agent  $j$  during the cycle starting at  $t$ . Thus,  $t_r = t + \tau_{ji}$ .

3) *Information Fusion and Decision-Making* After the communications, the ego vehicle would aggregate all available information  $\{\mathcal{M}_{ji}^t\}_{i \cup \mathcal{N}_i^t}$ <sup>6</sup> to derive fused features  $\tilde{\mathcal{F}}_i^{t_r}$

$$\tilde{\mathcal{F}}_i^{t_r} = \Phi_{\text{fuse}}(\{\mathcal{Z}_{ji}^{t_r} \odot \mathcal{M}_{ji}^t\}_{i \cup \mathcal{N}_i^t}) \in \mathbb{R}^{H \times W \times D}, \quad (8)$$

where  $\Phi_{\text{fuse}}$  is implemented with a feed-forward network and  $\mathcal{Z}_{ji}^{t_r} = \Phi_{\text{MHA}}(\mathcal{F}_i^t, \mathcal{M}_{ji}^t, \mathcal{M}_{ji}^t) \odot \mathcal{C}_j^t \in \mathbb{R}^{H \times W}$  indicates a scale-dot product attention generated with per-location multi-head attention  $\Phi_{\text{MHA}}$ . Next, by decoding the fused feature  $\tilde{\mathcal{F}}_i^{t_r}$  through a predefined decoder  $\Phi_{\text{decoder}}$  as

$$\tilde{\mathcal{H}}_i^{t_r}, \tilde{\mathcal{B}}_i^{t_r} = \Phi_{\text{decoder}}(\tilde{\mathcal{F}}_i^{t_r}) \in \mathbb{R}^{H \times W \times C}, \mathbb{R}^{H \times W \times 8C}, \quad (9)$$

where  $\tilde{\mathcal{H}}_i^{t_r}$  and  $\tilde{\mathcal{B}}_i^{t_r}$  represents the heatmap and bounding box regression map obtained with fused semantic information  $\tilde{\mathcal{F}}_i^{t_r}$ , respectively. 3D objects are then detected via non-maximum suppression [42] and then rasterized into a binary BEV occupancy map  $\mathcal{O}_i^{t_r}$ . Using  $T_d$ -length historical occupancy maps  $\{\mathcal{O}_i^k\}_{k=t_r-T_d, t_r}$  as well as the navigation information  $D_i^{t_r}$ , the ego vehicle leverages a learnable planner  $\Phi_{\text{plan}}$  encompassing a MotionNet [43] encoder, a goal encoder and corresponding waypoint decoder [4] to generate a driving plan consisting a series of waypoints  $\mathcal{W}_i^{t_r}$ . Mathematically, it can be described as

$$\mathcal{W}_i^{t_r} = \Phi_{\text{plan}}(\{\tilde{\mathcal{H}}_i^{t_r}, \tilde{\mathcal{B}}_i^{t_r}\}_{k=1}^{T_d}, \tilde{\mathcal{F}}_i^{t_r}, D_i^{t_r}) \in \mathbb{R}^{2 \times T_f}. \quad (10)$$

<sup>5</sup>Notably, due to the low-dimensional nature in BSMs, the latency for transmitting BSMs is assumed to be negligible relative to that for transmitting high-dimensional semantics  $\mathcal{M}_{ji}^t$  (i.e.,  $\tau_{ji}$ ).

<sup>6</sup>For simplicity of representation, we denote  $\mathcal{M}_{ii}^t = \mathcal{F}_i^t$  and  $\tau_{ii} = 0$ .

The optimal driving action  $\mathcal{A}_i^{t_r}$ , comprising steering, throttle, and brake commands, is then determined via lateral and longitudinal Proportional–Integral–Derivative (PID) controllers  $\Phi_{\text{controller}}$  as

$$\mathcal{A}_i^{t_r} = \Phi_{\text{controller}}(\mathcal{W}_i^{t_r}) \in [0, 1]^2 \cup \{0, 1\}^1. \quad (11)$$

### B. Problem Formulation

This paper aims to maximize the achievable driving performance through calibrated pragmatic communications. Particularly, the PragComm-based V2X-AD problem can be consistently formulated as

$$\begin{aligned} \max_{\theta, \eta} \sum_{i=1}^N \mathcal{E} \left[ \mathcal{W}_i^{t_r}, \Phi_{\text{plan}} \left( \Phi_{\text{percep}}(X_i^t, \{\mathcal{M}_{ji}^t\}_{\mathcal{N}_i^t}) \right) \right], \\ \text{s.t. } \mathcal{M}_{ji}^t = \Phi_{\text{process}}(\mathcal{F}_j^t, \mathcal{H}_i^t), \\ \left| \mathcal{M}_{ji}^t \right| \leq b_{ji} * \Delta\tau \text{ for } j \in \mathcal{N}_i^t, \end{aligned} \quad (12)$$

where  $\Phi_{\text{percep}}$  represents all involved perception-related DNNs in Eqs. (1) to (9). Specially,  $\Phi_{\text{process}}$  corresponds to the DNN-based PragComm components outlined in Eqs. (4) and (5), and the operator  $\mathcal{E}(\cdot)$  indicates metrics (e.g., Driving Score (DS), Route Completion (RC), and Infraction Score/Penalty (IS) [44]) in the driving scenarios, considering both safety rate and traffic efficiency. While the request map, as derived in Eq. (4), provides an intuitive foundation, it lacks task-specific optimization, such as the prioritization of information relevant to navigation information  $D_i^{t_r}$  [1], route planning [24], or salient objects [5], [45]. Even worse, the analyses presented in Appendix illustrate that, under ideal channel conditions, communication resources are insufficient to achieve latency-free communications, even for extremely compressed messages. On the other hand, for the highly volatile AD environment, due to the existence of computation and communications latency  $\tau_{ji}$ , the currently available observations in Eq. (5) might become outdated at time  $t_r$ . Instead, it favors by directly transmitting the forecast semantic features, predicted at time  $t$ , to complement the possible impact of latency  $\tau_{ji}$ . Nevertheless, although the estimation of the overall latency  $\tilde{\tau}_{ji}$  is achievable through a synchronization mechanism as in Section III-A2, the prediction of high-dimensional  $\mathcal{F}_j^t$  might impose a significant computational burden on the mobile device. Therefore, beyond simple information compression,  $\Phi_{\text{process}}$  (particularly Eq. (5)) shall be carefully investigated to effectively incorporate predicted background vehicle information at the expense of reduced computational overhead and minimal communications.

## IV. SELECT2DRIVE: DRIVING-ORIENTED COLLABORATIVE PERCEPTION

In this section, we introduce a Select2Drive framework that prioritizes the communications of decision-critical, timely content into the collaborative driving process. To obtain computationally efficient prediction, we reformulate it as a dimensionality reduction-based reconstruction problem and devise a DPP to extract the inherent transformation  $\vec{\mathcal{H}}_j^{t_r}$ , which represents the motion flow of objects from  $\mathcal{F}_j^t$  to  $\mathcal{F}_j^{t_r}$ ,

and subsequently infer  $\mathcal{F}_j^{t_r}$  from an affine approximation of  $\mathcal{F}_j^t$ . Furthermore, to ensure that improvements in perception performance consistently translate to enhanced outcomes in offline driving simulations, we design the message-packing mechanism (i.e., APC) on top of DPP.

### A. Distributed Predictive Perception (DPP)

As illustrated in Fig. 4, instead of directly predicting  $\vec{\mathcal{H}}_j^{t_r}$  from high-level semantics  $\mathcal{F}_j^t$ , which exhibits significant sensitivity to continuous latency  $\tau_{ji}$  [43], [46], we first down-sample the semantics  $\mathcal{F}_j^t, \mathcal{F}_j^{t_r}$  to low-level heatmap  $\mathcal{H}_j^t, \mathcal{H}_j^{t_r}$  with the decoder  $\Phi_{\text{decoder}}$  in Eq. (2). As mentioned earlier, due to the temporary unavailability of  $\mathcal{H}_j^{t_r}$ , we leverage a video prediction-inspired *iterative prediction* method to learn a predicted version  $\hat{\mathcal{H}}_j^{t_r}$ . Next, we introduce a *motion-aware affine transformation* mechanism to extract motion information  $\vec{\mathcal{H}}_j^{t_r} \in \mathbb{R}^{H \times W \times 2}$ , which correspond to the 2-dimensional positional shifts  $(\Delta x, \Delta y)$  for every object initially located at  $(x, y)$ .

1) *Iterative Prediction* We discretize the estimated latency  $\tilde{\tau}_{ji}$  into discrete steps  $n_{ji}^t = \lfloor \tilde{\tau}_{ji} / \tau \rfloor$ . Thus,  $t_r = t + n_{ji}^t \times \tau$ , consistent with the decision-making cycle  $\tau$  in Section III-A2. We iteratively generate a heatmap sequence  $\{\hat{\mathcal{H}}_j^{t+\tau}, \dots, \hat{\mathcal{H}}_j^{t_r}\}$  through  $n_{ji}^t$  steps as

$$\hat{\mathcal{H}}_j^{t+\tau}, \dots, \hat{\mathcal{H}}_j^{t_r} \xrightarrow[\text{for } n_{ji}^t]{\text{iteratively}} \Phi_{\text{DMVFN}}(\mathcal{H}_j^{t-\tau}, \mathcal{H}_j^t), \quad (13)$$

while use  $\hat{\mathcal{H}}_j^{t_r}$  to approximate  $\vec{\mathcal{H}}_j^{t_r}$ . To enable precise heatmap prediction with minimal computational overhead—thereby incurring trivial additional delays in  $\tau_{ji}^{\text{asyn}}$ —we comprehensively evaluate the State-Of-The-Art (SOTA) video prediction architectures, summarized in Table III, and prefer the DMVFN model [47] due to its superior balance between computational efficiency and predictive accuracy.

As depicted in Fig. 4, to ensure remarkable performance in resource-constrained settings, the DMVFN employs  $K = 9$  Multi-scale Voxel Flow Blocks (MVFBs) coupled with a dynamic routing module. Particularly, to effectively capture large-scale motion while maintaining spatial fidelity, each MVFB  $k \in \{1, \dots, K\}$  incorporates a dual-branch network structure, encompassing a motion path and a spatial path, to downsample the inputs by a scaling factor  $S^k$  for a larger receptive field while preserving fine-grained spatial details [53]. Subsequently, the outputs from both paths are concatenated to predict the voxel flow  $\mathcal{V}_j^k$ , which is then applied through backward warping [54] to generate a synthesized frame  $\hat{\mathcal{H}}_j^k$ .

Without loss of generality, taking the example of inputting  $(\mathcal{H}_j^{t-\tau}, \mathcal{H}_j^t)$ , each MVFB  $k$  is achieved by processing these two historical frames, a synthesized frame  $\hat{\mathcal{H}}_j^{k-1}$  and the voxel flow  $\mathcal{V}_j^{k-1}$  generated by the  $k-1$  MVFB block. Thus, we have

$$\hat{\mathcal{H}}_j^k, \mathcal{V}_j^k = \Phi_{\text{MVFB}}^k(\mathcal{H}_j^{t-\tau}, \mathcal{H}_j^t, \hat{\mathcal{H}}_j^{k-1}, \mathcal{V}_j^{k-1}, S^k). \quad (14)$$

When  $k = 1$ ,  $\hat{\mathcal{H}}_j^0$  and  $\mathcal{V}_j^0$  are set to zero.

On the other hand, the routing module is designed to dynamically balance the activation of each MVFB block, enabling adaptive selection according to the input variability.

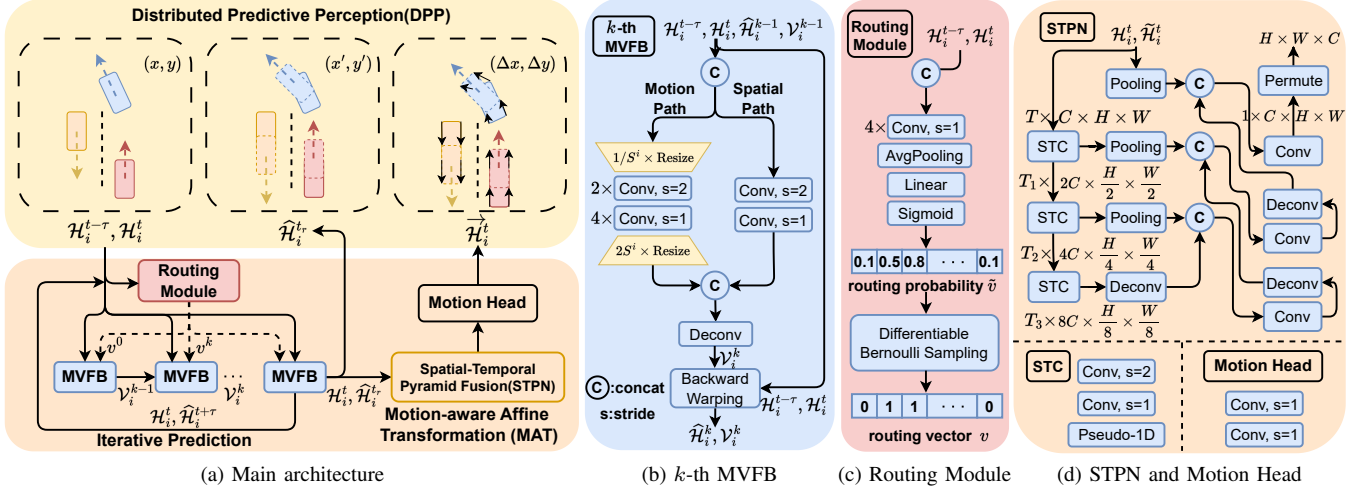


Fig. 4: Overview of the proposed DPP framework.

TABLE III: Parameters and Computational Overhead of Major Modules

Module	Params	FLOPs	Duty
DMVFN [47]	3.6 M	2.1 G	Forecast Future Confidence Map in $\Phi_{\text{DMVFN}}$
PredRNN++ [48]	24.6 M	169.8 G	
TAU [49]	38.7 M	85.0 G	
MAU [46]	10.5 M	29.1 G	
PhyDNet [50]	5.8 M	80.7 G	
PointPillar [51]	8.2 M	119 G	Extract Semantic Features in $\Phi_{\text{encoder}}, \Phi_{\text{decoder}}$
MotionNet [43]	1.7 M	10.2 G	Motion perception in $\Phi_{\text{MAT}}, \Phi_{\text{plan}}$
SDPA [52]	0.007 M	0.29 G	Fuse Intermediate Features in $\Phi_{\text{fuse}}$

<sup>1</sup> The statistics are collected during single-step driving scenarios with one-to-one communications.

<sup>2</sup> In terms of model lightness and faster decision-making efficiency, DMVFN is preferred.

Contingent on a lightweight DNN, the routing module is optimized using Differentiable Bernoulli Sampling (DBS), so as to prevent the routing module from converging to trivial solutions (e.g., consistently activating or bypassing specific blocks). Specifically, DBS incorporates Gumbel-Softmax [55] to determine the selection  $v^k \in \{0, 1\}$  of  $k$ -th MVFB through a stochastic classification task governed by  $\tilde{v}^k$  as

$$v^k = \frac{\exp\left(\frac{1}{\beta}(\tilde{v}^k + G_k)\right)}{\exp\left(\frac{1}{\beta}(\tilde{v}^k + G_k)\right) + \exp\left(\frac{1}{\beta}(2 - \tilde{v}^k - G_k)\right)}, \quad (15)$$

where  $G_k \in \mathbb{R}$  follows the Gumbel(0,1) distribution. The temperature parameter  $\beta$  starts with a high value to allow exploration of all possible paths and gradually decreases to approximate a one-hot distribution, ensuring effective and controllable routing. To ensure the participation of DBS in gradient computation during end-to-end training, the Straight-Through Estimator (STE) [56], which approximates the discrete sampling process in the backward pass, can be employed to further maintain compatibility with standard gradient descent optimization. In summary, the prediction process for the

$k$ -th MVFB is formulated as

$$\hat{\mathcal{H}}_j^k, \mathcal{V}_j^k = \begin{cases} \Phi_{\text{MVFB}}^k(\mathcal{H}_j^{t-\tau}, \mathcal{H}_j^t, \hat{\mathcal{H}}_j^{k-1}, \mathcal{V}_j^{k-1}, S^k), & v^k = 1; \\ \hat{\mathcal{H}}_j^{k-1}, \mathcal{V}_j^{k-1}, & v^k = 0. \end{cases} \quad (16)$$

To enhance the video prediction model's capacity for capturing dynamic information in traffic flow scenarios within the original training framework, we combine the standard  $\ell_1$  loss, which controls the contribution of each stage and regulated by a discount factor  $\gamma$ , with the VGG loss  $\mathcal{L}_{\text{Vgg}}$  [57] with a weight  $\varepsilon$ . The VGG loss revolves around leveraging the feature extraction capabilities of pre-trained VGG networks to quantify perceptual differences between images. Mathematically,

$$\mathcal{L}_{\text{DMVFN}} = \sum_{k=1}^n \gamma^{n-k} \ell_1(\mathcal{H}_j^{t+\tau}, \hat{\mathcal{H}}_j^k) + \varepsilon \mathcal{L}_{\text{Vgg}}, \quad (17)$$

where  $\mathcal{L}_{\text{Vgg}} = \sum_{m=1}^M \gamma_m \sum_{h,w,c=1}^{H_m, W_m, C_m} \frac{1}{H_m W_m C_m} (\phi_m(\mathcal{H}_j^{t+\tau})_{h,w,c} - \phi_m(\hat{\mathcal{H}}_j^{t+\tau})_{h,w,c})^2$ . Here,  $M = 5$  indicates the number of VGG layers we chose in the off-the-shelf VGG-19 network [57]. At the  $m$ -th layer,  $\phi_m(\zeta)$  refers to the feature representation of input  $\zeta$  and contributes to total loss with corresponding weight  $\gamma_m$ , and  $\phi_m(\zeta)_{h,w,c}$  specifies the value of the feature map at the  $h$ -th row,  $w$ -th column, and  $c$ -th channel for the input  $\zeta$  [57].  $H_m$ ,  $W_m$ , and  $C_m$  represent the height, width

and channel count of the feature map at the  $m$ -th layer, respectively.

2) *Motion-aware Affine Transformation (MAT)* Building upon the foundational work of [43],  $\Phi_{\text{MAT}}$  computes the motion prediction flow  $\vec{\mathcal{H}}_j^{t_r}$ , which explicitly encodes relative positional shifts between  $\mathcal{H}_j^t$  and  $\hat{\mathcal{H}}_j^{t_r}$ .

$$\vec{\mathcal{H}}_j^{t_r} = \Phi_{\text{MAT}}(\mathcal{H}_j^t, \hat{\mathcal{H}}_j^{t_r}), \quad (18)$$

As depicted in Fig. 4, the architecture of  $\Phi_{\text{MAT}}$  consists of two primary components: a Spatial-Temporal Pyramid Network (STPN) and a motion head, implemented by a two-layer 2D convolution module. The STPN is designed to extract multi-scale spatio-temporal features through its Spatial-Temporal Convolution (STC) block. The STC integrates standard 2D convolutions with a pseudo-1D convolution, which serves as a degenerate 3D convolution with kernel size  $T_m \times 1 \times 1$ , where  $\{T_m\}_{m=1,2,3}$  corresponds to the temporal dimension, enabling efficient feature extraction across both spatial and temporal dimensions. Spatially, the STPN computes feature maps at multiple scales with a scaling factor of 2, while temporally, it progressively reduces the temporal resolution to capture hierarchical temporal semantics. Following this, global temporal pooling and a feature decoder with lateral connections and upsample layers are employed to aggregate and refine the extracted temporal features, ensuring robust motion representation.

To precisely estimate the motion flow  $\vec{\mathcal{H}}_j^{t_r}$ , the loss function for  $\Phi_{\text{MAT}}$  is defined using the smooth  $\ell_1$  loss as

$$\mathcal{L}_{\text{MAT}} = \left\| \sum_k \sum_{(x,y),(x',y') \in o_k} f_A \left( f_\Delta(\vec{\mathcal{H}}_{(x,y)}^t, \vec{\mathcal{H}}_{(x',y')}^{t_r}) \right) - \vec{\mathcal{H}}_j^{t_r} \right\|, \quad (19)$$

where  $f_\Delta(\vec{\mathcal{H}}_{(x,y)}^t, \vec{\mathcal{H}}_{(x',y')}^{t_r}) \in \mathbb{R}^2$  represents the aggregated motion (i.e.,  $(\Delta x, \Delta y) = (x', y') - (x, y)$ ) of object  $k$  within instance  $o_k$  over the interval  $[t, t_r]$ , which is derived through grid-level comparisons between the Ground-Truth (GT) heatmaps  $\vec{\mathcal{H}}_i^t$  and  $\vec{\mathcal{H}}_i^{t_r}$  [43]. The operator  $f_A(\cdot)$  indicates a simple affine operation to map the increment  $(\Delta x, \Delta y)$  to the  $x$ -th column,  $y$ -th row into a  $H \times W$  matrix. Subsequently, the transformation of the semantic feature  $\mathcal{F}_j^t$  can be directly performed with the help of motion flow  $\vec{\mathcal{H}}_j^{t_r}$  as

$$\hat{\mathcal{F}}_j^{t_r}(x, y) = \mathcal{F}_j^t \left[ x + \vec{\mathcal{H}}_j^{t_r}(x, y, 0), y + \vec{\mathcal{H}}_j^{t_r}(x, y, 1) \right]. \quad (20)$$

### B. AoIm-based Pragmatic Communications

To address driving-related information within the PragComm procedure, we initiate by generating the request map  $\mathcal{R}_i^t$ . Given the inherent ambiguity of relying solely on navigation information  $D_i^{t_r}$  [58], the request map is constructed as a Gaussian distribution centered on the nearest waypoint  $(W_x, W_y)$  within prior waypoint plan  $\mathcal{W}_i^{t_r - \tau}$ , inspired by [45].

The formulation is given by:

$$\mathcal{R}_i^t(x, y) = \frac{1}{\sigma_F \sqrt{2\pi}} \exp \left( -\frac{(x - W_x)^2 + (y - W_y)^2}{2\sigma_F^2} \right), \quad (21)$$

where  $\sigma_F$ , termed the *Focus Radius*, is a hyperparameter controlling the width of the Gaussian distribution.

With the assistance of DPP, we further emphasize the dynamic information during message packing by computing  $\Delta \mathcal{C}_j^t(x, y) = \left| \tilde{\mathcal{C}}_j^t(x, y) - \mathcal{C}_j^t(x, y) \right|$  as an alert signal, which is proved to be practical in prior works [6], [10]. The message  $\mathcal{M}_{ji}^t$  is then packed as:

$$\mathcal{M}_{ji}^t = \hat{\mathcal{F}}_j^{t_r} \times \mathcal{P}_{ji}^t, \quad (22)$$

where  $\mathcal{P}_{ji}^t = \mathbf{1} \left( \max \left( \mathcal{R}_i^t \odot \tilde{\mathcal{C}}_j^t, \Delta \mathcal{C}_j^t / n_{ji}^t \right) \geq p_{\text{thre}} \right)$ . Subsequently, the information delivery, fusion and decision-making procedures can be conducted as in Section III-A3. In summary, Select2Drive can be executed as in Algorithm 1.

### C. Training Methods

In order to train the DNNs in Select2Drive, we assume the existence of a dataset  $\mathcal{T} = \{\xi_k\}_{k=0 \dots N}$ , which comprises trajectories  $\xi_k = \{(X_i^t, \mathcal{S}_i^{t_r}, \overline{\mathcal{W}}_i^{t_r})\}_{t=0 \dots T}$  representing sequences of state-action pairs, with actions  $\overline{\mathcal{W}}_i^{t_r} = \pi_E(\mathcal{S}_i^{t_r})$  derived from an expert policy  $\pi_E$ , where the real state  $\mathcal{S}_i^{t_r} = (\vec{\mathcal{H}}_i^t, \vec{\mathcal{B}}_i^t, D_i^{t_r})$ . The training process is structured around two interconnected parts (i.e., the perception-related DNN and the planning policy). For the former part, a  $\eta$ -parameterized DNN  $\Phi_{\text{percep}}$ , which encompasses the encoder  $\Phi_{\text{encoder}}$ , decoder  $\Phi_{\text{decoder}}$ , fuser  $\Phi_{\text{fuse}}$  as well as the incorporated intermediate DNNs, especially DMVFN and MAT in DPP, is learned through minimizing the center-point perception loss [59] through supervised learning,

$$\min_{\eta} \mathcal{L}(\eta) = \mathbb{E}_{(X_i^t, \mathcal{S}_i^{t_r}) \in \mathcal{T}} [(\tilde{\mathcal{S}}_i^{t_r} - \mathcal{S}_i^{t_r})^2] + \mathcal{L}_{\text{DMVFN}} + \mathcal{L}_{\text{MAT}}, \quad (23)$$

where  $\tilde{\mathcal{S}}_i^{t_r} = (\tilde{\mathcal{H}}_i^{t_r}, \tilde{\mathcal{B}}_i^{t_r}, D_i^{t_r})$  represents the estimated state.

On the other hand, the latter planning policy DNN  $\Phi_{\text{plan}}$  parameterized by  $\theta$  is trained using IL to minimize the  $l_2$ -norm deviation [60] between the low-level planning strategies and the expert policy  $\pi_E$  as

$$\min_{\theta} \mathcal{L}(\theta) = \mathbb{E}_{(\mathcal{S}_i^{t_r}, \overline{\mathcal{W}}_i^{t_r}) \in \mathcal{T}} [(\mathcal{W}_i^{t_r} - \overline{\mathcal{W}}_i^{t_r})^2] \quad (24)$$

where  $\mathcal{W}_i^{t_r} = \Phi_{\text{plan}}(\tilde{\mathcal{S}}_i^{t_r}, \tilde{\mathcal{F}}_i^{t_r})$  represents the waypoint plan using the estimated state  $\tilde{\mathcal{S}}_i^{t_r}$  along with fused semantic features  $\tilde{\mathcal{F}}_i^{t_r}$  given by the perception-related DNN with converged parameters  $\eta$ . Since APC masks irrelevant information in Eq. (21), the planning model would be separately fine-tuned.

## V. EXPERIMENTAL RESULTS AND DISCUSSIONS

### A. Experimental Settings

In this section, we evaluate the performance of Select2Drive in a high-fidelity environment based on CARLA [2] simulator,

<sup>7</sup>The occupancy map  $\mathcal{O}_i^{t_r}$  is derived through a non-trainable suppression mechanism and rasterization process applied to  $\tilde{\mathcal{S}}_i^{t_r}$ .



**Algorithm 1: Select2Drive**


---

**Input:** Raw sensor data and last planned waypoints  $\{X_i^t, \mathcal{W}_i^{t_r-\tau}\}_{i \in \mathcal{U} \cup \mathcal{N}_i^t}$  of ego  $i$  and its neighboring agents  $j \in \mathcal{N}_i^t$ ;

**Output:** Next driving action for each agent  $\{\mathcal{A}_i^{t_r}\}_{i \in \mathcal{U} \cup \mathcal{N}_i^t}$

- 1 **for** each agent  $i$  **do**
- 2     Generate intermediate semantic features  $\mathcal{F}_i^t$  along with solo-perception results  $\mathcal{H}_i^t, \mathcal{B}_i^t$  based on  $X_i^t$  using Eqs. (1)(2);
- 3     Exchange request map  $\mathcal{R}_i^t$  based on prior driving plan  $\mathcal{W}_i^{t_r-\tau}$  using Eq. (21) and estimate latency  $\tilde{\tau}_{ji}$  of sending message to neighbor  $j \in \mathcal{N}_i^t$ ;
- 4     **for** neighboring agent  $\mathcal{N}_i^t$  **do**
- 5          $n_{ji}^t \leftarrow \lfloor \tilde{\tau}_{ji} / \tau \rfloor$ ;
- 6         Predict future heatmap  $\hat{\mathcal{H}}_j^{t_r}$  based on historical information  $\mathcal{H}_j^{t_r-\tau}, \mathcal{H}_j^t$  through  $n_{ji}^t$  iterations of DMVFN in Eq. (16);
- 7         Extract motion flow  $\vec{\mathcal{H}}_j^{t_r}$  between  $\mathcal{H}_j^t$  and  $\hat{\mathcal{H}}_j^{t_r}$  with MAT in Eq. (18) ;
- 8         Apply affine approximation  $\vec{\mathcal{H}}_j^{t_r}$  on semantic features  $\mathcal{F}_j^t$  to estimate high-level semantic information  $\hat{\mathcal{F}}_j^{t_r}$  with Eq. (20) ; ▷ DPP
- 9         Send packed Message  $\mathcal{M}_{ji}^t$  based on  $\hat{\mathcal{F}}_j^{t_r}$  and confidence map  $\mathcal{C}_i^t$  generated with Eq. (4) using Eq. (22) ; ▷ APC
- 10     **end**
- 11     Fuse received message  $\{\mathcal{M}_{ji}^t\}_{i \in \mathcal{U} \cup \mathcal{N}_i^t}$  and ego information  $\mathcal{F}_i^t$  to obtain collaborated semantics  $\tilde{\mathcal{F}}_i^{t_r}$  using Eq. (8);
- 12     Generate next driving plan  $\mathcal{W}_i^{t_r}$  and make driving decision  $\mathcal{A}_i^{t_r}$  based on  $\tilde{\mathcal{F}}_i^{t_r}$  using Eqs. (9)(11);
- 13 **end**
- 14 **return** Next action  $\{\mathcal{A}_i^{t_r}\}_{i \in \mathcal{U} \cup \mathcal{N}_i^t}$

---

which facilitates sensor rendering and the computation of physics-based updates to the world state. It adheres to the ASAM OpenDRIVE standard [61] for defining road networks and urban environments. Table IV outlines the principal experimental parameters, with communications-related parameters primarily mentioned in [26]. The overall latency  $\tau_{ji}$  is simulated as assumed bandwidth constraints in [35] and C-V2X [36] as in Section III-A2. Since DSRC-based transmission meets hidden node issues, which can lead to packet collisions [8], are modeled by constraining  $\tau_{ji}^{\text{pr}}$  with limited bandwidth, while  $\tau_{ji}^{\text{net}} = 0$  due to its direct communication nature. Differently, in C-V2X, the impact of  $\tau_{ji}^{\text{net}}$  is more pronounced due to the possible handover procedures, and  $\tau_{ji}^{\text{tx}}$  is assumed to be fixed latency. As the V2X-AD framework naturally divides into perception and subsequent driving tasks, we evaluate our proposed method across two distinct stages.

- *For planning policy*, we simulate the closed-loop driving task through both offline expert trajectory replication and online route completion tasks. Offline simulations emulate expert-driven trajectories within static datasets,

TABLE IV: Mainly used parameters in this paper.

Parameter	Value
<b>DSRC-based transmission</b>	
Interval $\Delta\tau$ for SCHI and CCHI	50 ms
Fixed Decision Interval $\tau$	100 ms
Allocated Bandwidth $b_{ji}$	1 ~ 20 MHz
Transmit Power $p_{ji}^{\text{tx}}$	23 dbm
Power of Noise $p_{ji}^{\text{noise}}$	-95 ~ -110dbm
Carrier Frequency $f_c$	5.9 GHz
<b>C-V2X-based transmission</b>	
Fixed transmission Latency $\tau_{ji}^{\text{pr}} + \tau_{ji}^{\text{net}}$	0 ~ 600 ms
<b>Shared Latency-related parameters</b>	
Asynchronous latency $\tau_{ji}^{\text{asyn}}$	-100 ~ 100 ms
Semantic Extraction Time $\tau_j^{\text{ext}}$	20 ~ 40 ms
Decision-Making Time $\tau_i^{\text{dm}}$	10 ~ 20 ms
<b>Hyperparameters</b>	
Height, Width, Channel $\{H, W, D\}$	[64, 192, 576]
Request Map Threshold $p_{\text{thre}}$	0.05
Focus Radius $\sigma_F$	15 m
Number of frames for planning $T_d$	5
Number of waypoints to plan $T_f$	10
Scaling factors $\{S^k\}_{k=1}^9$	[4, 4, 4, 2, 2, 2, 1, 1, 1]
Discount factor $\gamma$ , VGG weight $\varepsilon$	0.8, 0.5
Index $\{m\}_M$ of VGG Layers and Corresponding weights $\{\gamma_m\}_M$	[2, 7, 12, 21, 30], [0.38, 0.21, 0.27, 0.18, 6.67]
Temporal factors in STPN $T_1, T_2, T_3$	[2, 2, 1]

utilizing Average Displacement Error (ADE) to quantify deviations between model predictions and expert trajectories. All decision-making policies are pre-trained on V2Xverse [1], while online tasks are tested on the 31 Town05 Short Routes in the CARLA Leaderboard [31] version 0.9.10, where the ego vehicle collaborates with the nearest RSUs. The baselines include an IL-based planner trained atop the collaborative perception frameworks outlined in [13], [16], [17], with the current SOTA collaborative driving method Codriving [1], recognized as an integration of [17] and the IL-based planner. Additionally, prominent single-agent end-to-end methodologies are also considered, such as TCP [24] and the SOTA Interfuser [4]. Consistent with [7], we adopt several key metrics such as DS, RC, and IS [44]. Particularly, RC is defined by the percentage of routes completed by the agent and indicates its ability to finish the assigned task, while IS is calculated as a geometric series that penalizes based on the severity and frequency of violations and reflects adherence to traffic rules. In addition, as the product of RC and IS, DS provides a weighted measure of route completion and compliance with traffic regulations.

- *For perception capability*, we leverage the V2Xverse dataset [1] for offline perception performance evaluation, since the dataset comprehensively incorporates RSUs

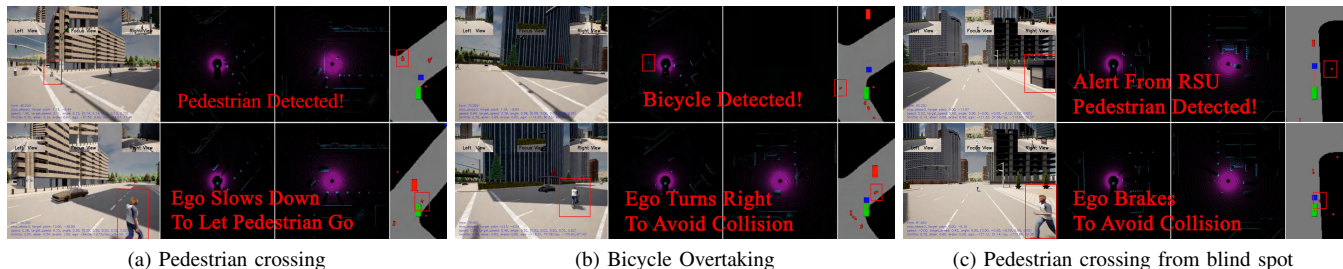


Fig. 5: Visualization for Closed-loop driving upon several classic scenarios. The visualization delineates the ego vehicle’s position with a green box, the planned trajectory with a red dot, detected obstacles as red squares, and the next waypoint along the route as a blue square.

TABLE V: Closed-Loop Driving Performance.

Method	Avg. Driving Score $\uparrow$	Avg. Route Completion (%) $\uparrow$	Avg. Infraction Penalty $\downarrow$	Collisions With Pedestrians $\downarrow$	Collisions With Vehicles $\downarrow$	Collisions With Layout $\downarrow$	Off-road Infractions $\downarrow$	Mean Speed $\uparrow$
No Communications								
<u>Interfuser</u> [4]	<u>35.372</u>	<u>79.254</u>	<u>0.434</u>	<u>0.052</u>	<u>0.492</u>	<u>0.568</u>	<u>0.223</u>	<u>0.586</u>
<u>TCP</u> [24]	<u>38.214</u>	<u>50.526</u>	<u>0.817</u>	<u>0.029</u>	<u>0.079</u>	<u>0.069</u>	<u>0.004</u>	<u>1.066</u>
<b>No Fusion</b>	<b>38.481</b>	<b>84.732</b>	<b>0.432</b>	<b>0.109</b>	<b>0.379</b>	<b>0.603</b>	<b>0.105</b>	<b>0.569</b>
Bandwidth = 20 MHz (uniform latency = 0ms)								
When2Com [16]	30.571	41.840	0.646	0.028	0.923	0.450	0.416	0.218
Where2Comm [17]	35.811	82.266	0.394	0.156	0.390	0.393	0.115	0.791
<u>Select2Col</u> [13]	<u>35.178</u>	<u>69.045</u>	<u>0.492</u>	<u>0.126</u>	<u>0.572</u>	<u>0.371</u>	<u>0.106</u>	<u>0.442</u>
<i>Select2Drive wo APC</i>	<i>40.991</i>	<i>82.535</i>	<i>0.411</i>	<i>0.148</i>	<i>0.447</i>	<i>0.404</i>	<i>0.126</i>	<i>0.978</i>
<b>Select2Drive</b>	<b>46.904</b>	<b>82.284</b>	<b>0.446</b>	<b>0.140</b>	<b>0.270</b>	<b>0.008</b>	<b>0.083</b>	<b>1.211</b>
Bandwidth = 10 MHz (uniform latency = 100ms)								
When2Com	29.915	43.725	0.632	0.051	0.953	0.410	0.385	0.257
<u>Where2Comm</u>	<u>33.704</u>	<u>48.560</u>	<u>0.651</u>	<u>0.054</u>	<u>0.640</u>	<u>0.351</u>	<u>0.115</u>	<u>0.668</u>
Select2Col	29.794	70.232	0.414	0.189	0.516	0.348	0.118	0.448
<i>Select2Drive wo APC</i>	<i>40.725</i>	<i>66.760</i>	<i>0.496</i>	<i>0.052</i>	<i>0.469</i>	<i>0.482</i>	<i>0.142</i>	<i>1.066</i>
<b>Select2Drive</b>	<b>45.062</b>	<b>81.157</b>	<b>0.456</b>	<b>0.117</b>	<b>0.310</b>	<b>0.376</b>	<b>0.095</b>	<b>0.976</b>
Bandwidth = 5 MHz (uniform latency = 200ms)								
When2Com	27.204	38.392	0.652	0.043	1.114	0.377	0.514	0.507
<u>Where2Comm</u>	<u>31.976</u>	<u>51.161</u>	<u>0.527</u>	<u>0.119</u>	<u>0.514</u>	<u>0.399</u>	<u>0.188</u>	<u>0.306</u>
Select2Col	28.391	64.284	0.447	0.096	0.586	0.345	0.137	0.486
<i>Select2Drive wo APC</i>	<i>38.853</i>	<i>54.574</i>	<i>0.627</i>	<i>0.044</i>	<i>0.626</i>	<i>0.340</i>	<i>0.331</i>	<i>0.860</i>
<b>Select2Drive</b>	<b>43.823</b>	<b>70.588</b>	<b>0.520</b>	<b>0.088</b>	<b>0.373</b>	<b>0.497</b>	<b>0.126</b>	<b>1.211</b>

<sup>1</sup> The best-performing results are highlighted in **bold**, the second-best are indicated in *italics*, and the third-best are marked with underlines.

compared to the widely used OPV2V dataset [62], extending beyond vehicle-to-vehicle (V2V) communications. The baseline methodologies include approaches like When2Com [16] and Where2Comm [17], as well as the SOTA Select2Col [13]. Additionally, a no-fusion baseline is included to evaluate performance in the absence of collaborative mechanisms. Following the evaluation metrics outlined in [13], the perception performance is measured using *Average Precision (AP) at Intersection over Union (IoU) thresholds of 0.3, 0.5, and 0.7* for vehicles, two-wheeled vehicles, and pedestrians, denoted as AP30, AP50, and AP70. To enhance clarity, the Compositd AP is a weighted sum of AP30, AP50, and AP70, with respective weights of 0.3, 0.3, and 0.4. Also, to

streamline representation, perception results for vehicles, bicycles, and pedestrians are merged with weights of 0.4, 0.4, and 0.2. As for communication volume, we calculate it as  $\log_2(H \times W \times D \times \|\mathcal{P}_{ji}^t\|_1 \times 32/8)$ .

## B. Qualitative Results

1) *Driving Task* Qualitatively, as illustrated in Fig. 5, the proposed approach effectively leverages PragComm-based driving critical information for emergent obstacle perception and timely collision avoidance.

Table V demonstrates a marked performance enhancement of 30.84% upon DS using the proposed methodology compared with the SOTA approach [1]. Under bandwidth constraints, the collaborative driving paradigm maintains a

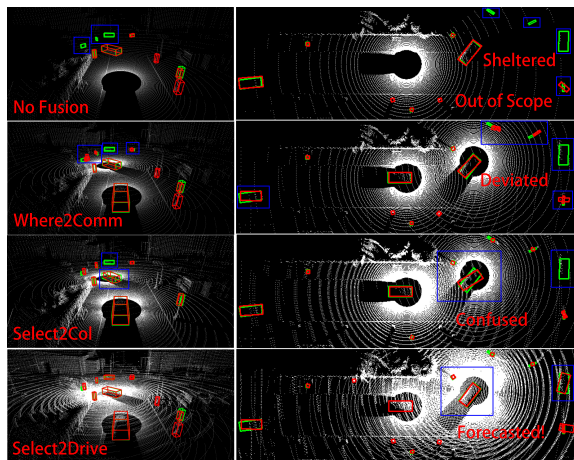


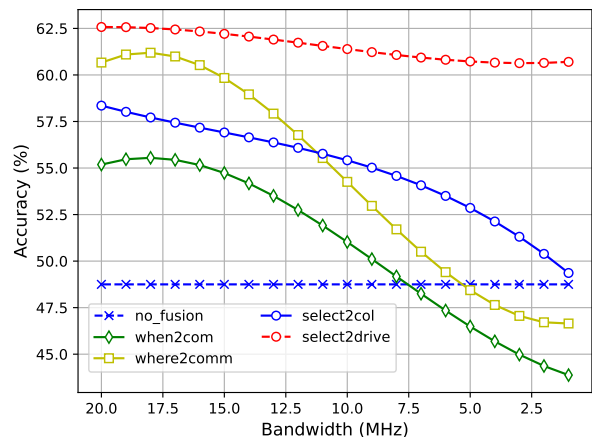
Fig. 6: Visualization of collaborative perception in bandwidth-constrained (5 MHz) scenarios. The red box illustrates the ego vehicle’s predicted positions for surrounding objects, whereas the green box indicates the GT positions of those objects.

14.68% DS advantage compared to the latest available single-agent SOTA TCP method [24]. Notable gains can be observed in RC (31.76% improvement) and IS (45.41% reduction). Ablation studies confirm the contribution of the APC methodology, yielding a 14.43% improvement in the DS and empirically validating our “less is more” hypothesis. Conversely, latency-agnostic methods [16], [17] exhibit significant performance degradation under high-latency conditions.

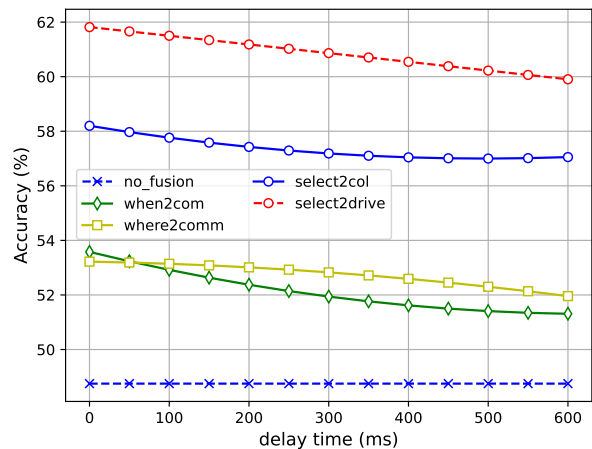
2) *Perception Performance* Fig. 6 presents qualitative findings. It can be observed that the predictive approach in Select2Drive facilitates the timely acquisition of projected data from surrounding vehicles, thus effectively addressing blind zone perception. Due to the neglect of latency, Where2Comm [17] employs outdated information aggregation, and consequently generates notable perceptual inaccuracies. Meanwhile, Select2Col [13] offers partial remediation, yet remains susceptible to blind zone perception loss stemming from temporal constraints.

Fig. 7 illustrates the perceptual performance across various methodologies under DSRC-based and C-V2X-based transmission scenarios. Under ideal communication conditions, a comprehensive multi-object perception evaluation indicates our method outperforms the other baselines. Meanwhile, in more realistic V2X scenarios, while existing methods [13], [16], [17] degrade to performance levels akin to non-communicative setups, DPP demonstrates sustained gains of 6.94% (10 MHz) and 3.64% (300 ms). Even under severely constrained bandwidth conditions, our method still maintains superior accuracy.

As illustrated in Fig. 8, DPP demonstrates robust stability in the presence of angular noise  $\sigma_r$ , which represents deviations in angular values ( $\sin \alpha, \cos \alpha$ ) in the coordinate system. Meanwhile, its performance is slightly compromised when subject to positioning noise  $\sigma_p$  representing inaccuracies in  $(x, y, z)$ . Nevertheless, under moderate noise conditions, our method achieves significant gains of 7.76% ( $\sigma_p = 0.1$ ), 9.10% ( $\sigma_r = 0.1$ ), and 7.69% ( $\sigma_p = \sigma_r = 0.1$ ) compared to non-



(a) DSRC-based Transmission.



(b) C-V2X-based Transmission.

Fig. 7: Quantitative analysis for the collaborative perception task under communication constraints.

collaborative perception schemes. Even in extreme rotation error scenarios ( $\sigma_p = 1.0$ ), it maintains a 2.70% improvement in accuracy against the no fusion method. This suggests that the approach possesses strong correction capabilities while relying heavily on precise positional information.

3) *Hyperparameter Research* As illustrated in Fig. 9, the hyperparameter  $p_{\text{thre}}$  in Eq. (21) predominantly regulates the stringency of message exchange. A higher value diminishes the volume of information involved in aggregation, potentially inducing a degradation in perception performance. To achieve an optimal trade-off between communication efficiency and perception accuracy, we empirically set  $p_{\text{thre}} = 0.05$ . This configuration yields a 2.65% enhancement in composite average precision (AP), accompanied by a marginal increase in communication overhead of 0.06 dB (4.33%). With the optimal  $p_{\text{thre}}$  determined through perception tasks, we further investigate the impact of  $\sigma_F$  in Eq. (22). A lower value of this hyperparameter enforces stricter filtering of content irrelevant to the driving task, thereby enhancing offline simulation performance during expert behavior imitation. However, in closed-loop driving scenarios, precise imitation of the expert with reduced information does not consistently yield improved real-world driving performance. Through extensive closed-

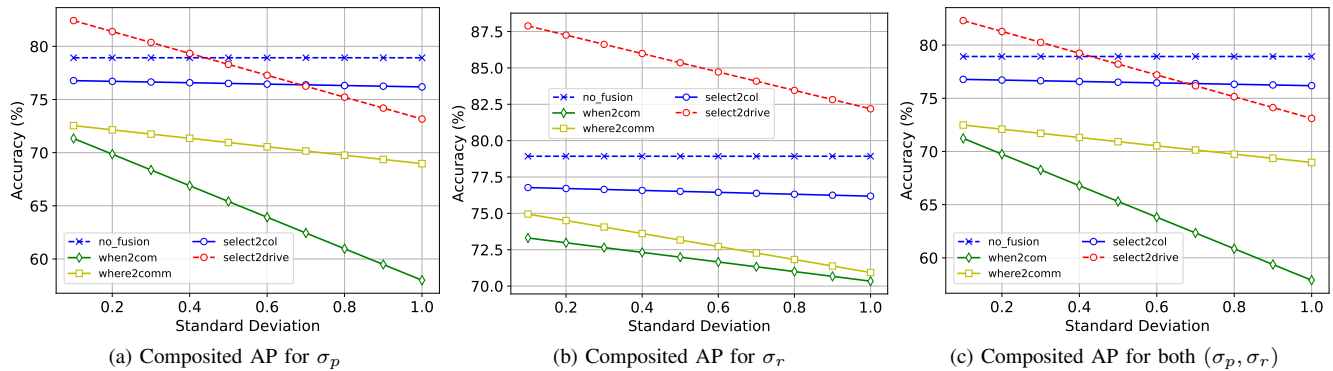


Fig. 8: Robustness of DPP to the vehicle pose noise in the perception task.

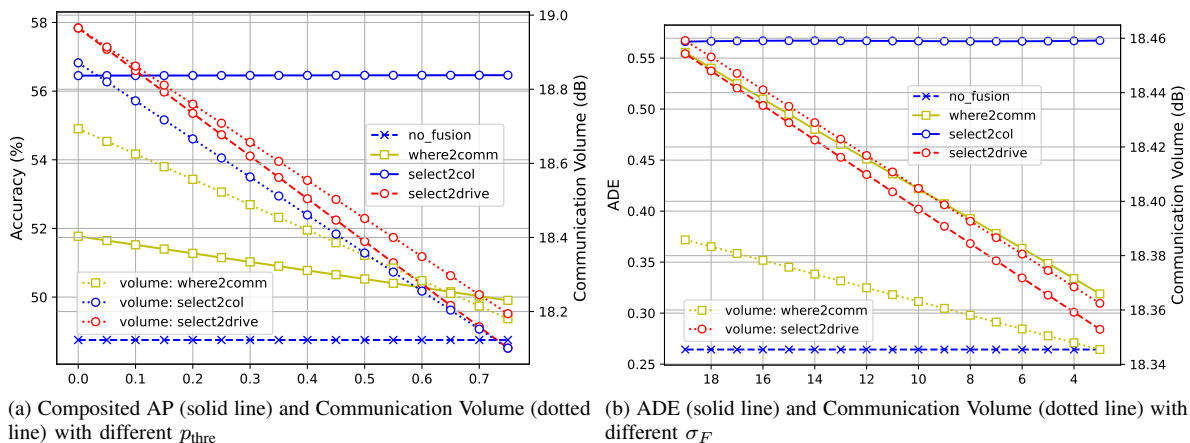


Fig. 9: Quantitative analysis on the influence of  $p_{\text{thre}}$  and  $\sigma_F$ .

loop driving experiments, we set  $\sigma_F$  to 15 to prevent artificially inflated performance metrics resulting from excessive communication reduction.

## VI. CONCLUSIONS

In this work, we have presented a PragComm-based real-time collaborative driving framework Select2Drive, which novelly comprises two key components (i.e. DPP and APC) to address the critical timeliness challenges in V2X-AD systems. In particular, the DPP algorithm integrates predictive modeling and motion-aware affine transformation to infer future high-dimensional semantic features, maintaining robust perception performance even under severe positioning noise or constrained communication scenarios. Simultaneously, APC enhances decision-making efficiency by restricting communications to critical regions and minimizing unnecessary data exchanges, thereby mitigating potential confusion in decision-making. Extensive evaluations have been conducted on both collaborative perception tasks and online closed-loop driving simulations. The experimental results demonstrate that our communication-efficient optimization framework is well-suited for real-time collaborative perception tasks, achieving significant performance improvements across a wide range of scenarios. In the future, we will explore integrating generative

models to enhance driving policy robustness across diverse scenarios.

## REFERENCES

- [1] G. Liu, Y. Hu, C. Xu, *et al.*, “Towards collaborative autonomous driving: Simulation platform and end-to-end system,” *arXiv preprint arXiv:2404.09496*, 2024.
- [2] A. Dosovitskiy, G. Ros, F. Codevilla, *et al.*, “CARLA: An open urban driving simulator,” in *Proceedings of the 1st Annual Conference on Robot Learning*, Mountain View, CA, USA, 2017.
- [3] D. Chen, B. Zhou, V. Koltun, *et al.*, “Learning by cheating,” in *Proceedings of the Conference on Robot Learning (CoRL)*, Auckland, New Zealand, 2020, pp. 66–75.
- [4] H. Shao, L. Wang, R. Chen, *et al.*, “Safety-enhanced autonomous driving using interpretable sensor fusion transformer,” *arXiv preprint arXiv:2207.14024*, 2022.
- [5] K. Renz, K. Chitta, O.-B. Mercea, *et al.*, “Plant: Explainable planning transformers via object-level representations,” in *Proceedings of the 6th Conference on Robot Learning*, Atlanta, GA, USA, 2023, pp. 459–470.
- [6] H. Shao, L. Wang, R. Chen, *et al.*, “Reasonnet: End-to-end driving with temporal and global reasoning,” in *2023 IEEE/CVF Conference on Computer Vision and Pattern Recognition (CVPR)*, Vancouver, BC, Canada, 2023, pp. 13 723–13 733.
- [7] P. S. Chib and P. Singh, “Recent advancements in end-to-end autonomous driving using deep learning: A survey,” *IEEE Transactions on Intelligent Vehicles*, vol. 9, no. 1, pp. 103–118, 2024.
- [8] R. Sedar, C. Kalalas, F. Vázquez-Gallego, *et al.*, “A comprehensive survey of V2X cybersecurity mechanisms and future research paths,” *IEEE Open Journal of the Communications Society*, vol. 4, pp. 325–391, 2023.

- [9] S. Liu, C. Gao, Y. Chen, *et al.*, “Towards vehicle-to-everything autonomous driving: A survey on collaborative perception,” *arXiv preprint arXiv:2308.16714*, 2023.
- [10] J. Cui, H. Qiu, D. Chen, *et al.*, “Coopernaut: End-to-end driving with cooperative perception for networked vehicles,” in *2022 IEEE/CVF Conference on Computer Vision and Pattern Recognition (CVPR)*, New Orleans, LA, USA, 2022, pp. 17 231–17 241.
- [11] S. U. Bhoover, A. Tugashetti, and P. Rashinkar, “V2X communication protocol in vanet for co-operative intelligent transportation system,” in *2017 International Conference on Innovative Mechanisms for Industry Applications (ICIMIA)*, Sydney, Australia, 2017, pp. 602–607.
- [12] X. Gu, G. Zhang, Y. Ji, *et al.*, “Intelligent surface aided D2D-V2X system for low-latency and high-reliability communications,” *IEEE Transactions on Vehicular Technology*, vol. 71, no. 11, pp. 11 624–11 636, 2022.
- [13] Y. Liu, Q. Huang, R. Li, *et al.*, “Select2col: Leveraging spatial-temporal importance of semantic information for efficient collaborative perception,” *IEEE Transactions on Vehicular Technology*, vol. 73, no. 9, pp. 12 556–12 569, 2024.
- [14] C. D. Alwis, A. Kalla, Q.-V. Pham, *et al.*, “Survey on 6G frontiers: Trends, applications, requirements, technologies and future research,” *IEEE Open Journal of the Communications Society*, vol. 2, pp. 836–886, 2021.
- [15] Y. Hu, X. Pang, X. Qin, *et al.*, “Pragmatic communication in multi-agent collaborative perception,” *arXiv preprint arXiv:2401.12694*, 2024.
- [16] Y.-C. Liu, J. Tian, N. Glaser, *et al.*, “When2com: Multi-agent perception via communication graph grouping,” in *2020 IEEE/CVF Conference on Computer Vision and Pattern Recognition (CVPR)*, Seattle, WA, USA, 2020, pp. 4105–4114.
- [17] Y. Hu, S. Fang, Z. Lei, *et al.*, “Where2comm: Communication-efficient collaborative perception via spatial confidence maps,” in *Advances in Neural Information Processing Systems (NeurIPS)*, New Orleans Convention Center, 2022, pp. 4874–4886.
- [18] S. Wei, Y. Wei, Y. Hu, *et al.*, “Asynchrony-robust collaborative perception via bird’s eye view flow,” in *Advances in Neural Information Processing Systems (NeurIPS)*, New Orleans, LA, USA, 2023, pp. 28 462–28 477.
- [19] Z. Lei, Z. Ni, R. Han, *et al.*, “Robust collaborative perception without external localization and clock devices,” in *2024 IEEE International Conference on Robotics and Automation (ICRA)*, Yokohama, Japan, 2024, pp. 7280–7286.
- [20] S. Reddy, A. Dragan, and S. Levine, “Pragmatic image compression for human-in-the-loop decision-making,” in *Advances in Neural Information Processing Systems (NeurIPS)*, Online, 2021, pp. 26 499–26 510.
- [21] D. Gündüz, F. Chiariotti, K. Huang, *et al.*, “Timely and massive communication in 6G: Pragmatics, learning, and inference,” *IEEE BITS the Information Theory Magazine*, vol. 3, no. 1, pp. 27–40, 2023.
- [22] Y. Lu, Y. Hu, Y. Zhong, *et al.*, “An extensible framework for open heterogeneous collaborative perception,” in *International Conference on Learning Representations (ICLR)*, Vienna Austria, 2024.
- [23] Q. Li, Z. Peng, H. Wu, *et al.*, “Human-AI shared control via policy dissection,” in *Advances in Neural Information Processing Systems (NeurIPS)*, New Orleans Convention Center, 2022, pp. 8853–8867.
- [24] P. Wu, X. Jia, L. Chen, *et al.*, “Trajectory-guided control prediction for end-to-end autonomous driving: A simple yet strong baseline,” in *Advances in Neural Information Processing Systems*, S. Koyejo, S. Mohamed, A. Agarwal, *et al.*, Eds., vol. 35. New Orleans, LA, USA: Curran Associates, Inc., 2022, pp. 6119–6132. [Online]. Available: [https://proceedings.neurips.cc/paper\\_files/paper/2022/file/286a371d8a0a559281f682f8fbf89834-Paper-Conference.pdf](https://proceedings.neurips.cc/paper_files/paper/2022/file/286a371d8a0a559281f682f8fbf89834-Paper-Conference.pdf)
- [25] S. So, J. Petit, and D. Starobinski, “Physical layer plausibility checks for misbehavior detection in V2X networks,” in *Proceedings of the 12th Conference on Security and Privacy in Wireless and Mobile Networks*, New York, NY, USA, 2019, pp. 84–93.
- [26] Y. Yao, B. Xiao, G. Wu, *et al.*, “Multi-Channel based Sybil Attack Detection in Vehicular Ad Hoc Networks using RSSI,” *IEEE Transactions on Mobile Computing*, vol. 18, no. 2, pp. 362–375, 2019.
- [27] H. Yu, Y. Tang, E. Xie, *et al.*, “Flow-based feature fusion for vehicle-infrastructure cooperative 3d object detection,” in *Advances in Neural Information Processing Systems (NeurIPS)*, New Orleans, LA, USA, 2023, pp. 34 493–34 503.
- [28] T.-Y. Tung, S. Kobus, J. P. Roig, *et al.*, “Effective Communications: A joint learning and communication framework for multi-agent reinforcement learning over noisy channels,” *IEEE Journal on Selected Areas in Communications*, vol. 39, no. 8, pp. 2590–2603, 2021.
- [29] —, “Context-aware Effective Communications,” in *2021 55th Asilomar Conference on Signals, Systems, and Computers*, California, USA, 2021, pp. 334–339.
- [30] S. Ross and D. Bagnell, “Efficient reductions for Imitation Learning,” in *Proceedings of the 13th International Conference on Artificial Intelligence and Statistics*, Chia Laguna Resort, Sardinia, Italy, 2010, pp. 661–668.
- [31] CARLA, “Carla leaderboard,” <https://leaderboard.carla.org/leaderboard/>.
- [32] C. Zhang, F. Steinhauser, G. Hinz, *et al.*, “Occlusion-aware planning for autonomous driving with vehicle-to-everything communication,” *IEEE Transactions on Intelligent Vehicles*, vol. 9, no. 1, pp. 1229–1242, 2024.
- [33] F. Codevilla, M. Müller, A. López, *et al.*, “End-to-end driving via conditional Imitation Learning,” in *2018 IEEE International Conference on Robotics and Automation (ICRA)*, Brisbane, Australia, 2018, pp. 4693–4700.
- [34] C. E. Shannon, “A mathematical theory of communication,” *The Bell System Technical Journal*, vol. 27, no. 3, pp. 379–423, 1948.
- [35] D. Jiang and L. Delgrossi, “IEEE 802.11p: Towards an international standard for wireless access in vehicular environments,” in *2008 IEEE Vehicular Technology Conference (VTC Spring)*, Singapore, 2008, pp. 2036–2040.
- [36] S. Chen, J. Hu, Y. Shi, *et al.*, “Vehicle-to-everything (V2X) services supported by lte-based systems and 5G,” *IEEE Communications Standards Magazine*, vol. 1, no. 2, pp. 70–76, 2017.
- [37] J. B. Kenney, “Dedicated short-range communications (DSRC) standards in the united states,” *Proceedings of the IEEE*, vol. 99, no. 7, pp. 1162–1182, 2011.
- [38] D. Garcia-Roger, E. E. González, D. Martín-Sacristán, *et al.*, “V2X support in 3GPP specifications: From 4G to 5G and beyond,” *IEEE Access*, vol. 8, pp. 190 946–190 963, 2020.
- [39] H. Noh, S. Hong, and B. Han, “Learning deconvolution network for semantic segmentation,” in *2015 IEEE International Conference on Computer Vision (ICCV)*, Santiago, Chile, 2015, pp. 1520–1528.
- [40] Q. Zhu, C.-X. Wang, B. Hua, *et al.*, *3GPP TR 38.901 Channel Model*, 2021, pp. 1–35.
- [41] S. Gyawali, S. Xu, Y. Qian, *et al.*, “Challenges and solutions for cellular based V2X communications,” *IEEE Communications Surveys and Tutorials*, vol. 23, no. 1, pp. 222–255, 2021.
- [42] A. Neubeck and L. Van Gool, “Efficient non-maximum suppression,” in *18th International Conference on Pattern Recognition (ICPR’06)*, vol. 3, Hong Kong, China, 2006, pp. 850–855.
- [43] P. Wu, S. Chen, and D. N. Metaxas, “Motionnet: Joint perception and motion prediction for autonomous driving based on bird’s eye view maps,” in *2020 IEEE/CVF Conference on Computer Vision and Pattern Recognition (CVPR)*, Seattle, WA, USA, 2020, pp. 11 382–11 392.
- [44] X. Jia, Z. Yang, Q. Li, *et al.*, “Bench2drive: Towards multi-ability benchmarking of closed-loop end-to-end autonomous driving,” *arXiv preprint arXiv:2406.03877*, 2024.
- [45] I. Kotseruba and J. K. Tsotsos, “Understanding and modeling the effects of task and context on drivers’ gaze allocation,” in *2024 IEEE Intelligent Vehicles Symposium (IV)*, Jeju, South Korea, 2024, pp. 1337–1344.
- [46] Z. Chang, X. Zhang, S. Wang, *et al.*, “Mau: A motion-aware unit for video prediction and beyond,” in *Advances in Neural Information Processing Systems*, vol. 34, Virtual, 2021, pp. 26 950–26 962. [Online]. Available: [https://proceedings.neurips.cc/paper\\_files/paper/2021/file/e25cfa90f04351958216f97e3efdbae9-Paper.pdf](https://proceedings.neurips.cc/paper_files/paper/2021/file/e25cfa90f04351958216f97e3efdbae9-Paper.pdf)
- [47] X. Hu, Z. Huang, A. Huang, *et al.*, “A dynamic multi-scale voxel flow network for video prediction,” in *2023 IEEE/CVF Conference on Computer Vision and Pattern Recognition (CVPR)*, Vancouver, BC, Canada, 2023, pp. 6121–6131.
- [48] Y. Wang, Z. Gao, M. Long, *et al.*, “Predrnn++: Towards a resolution of the deep-in-time dilemma in spatiotemporal predictive learning,” in *Proceedings of the 35th International Conference on Machine Learning*, Stockholm, Sweden, 2018, pp. 5123–5132.
- [49] C. Tan, Z. Gao, L. Wu, *et al.*, “Temporal attention unit: Towards efficient spatiotemporal predictive learning,” in *2023 IEEE/CVF Conference on Computer Vision and Pattern Recognition (CVPR)*, Vancouver, BC, Canada, 2023, pp. 18 770–18 782.
- [50] V. L. Guen and N. Thome, “Disentangling physical dynamics from unknown factors for unsupervised video prediction,” in *2020 IEEE/CVF Conference on Computer Vision and Pattern Recognition (CVPR)*, Seattle, WA, USA, 2020, pp. 11 471–11 481.
- [51] A. H. Lang, S. Vora, H. Caesar, *et al.*, “Pointpillars: Fast encoders for object detection from point clouds,” in *2019 IEEE/CVF Conference on Computer Vision and Pattern Recognition (CVPR)*, Long Beach, CA, USA, 2019, pp. 12 689–12 697.

- [52] A. Vaswani, N. Shazeer, N. Parmar, *et al.*, “Attention is all you need,” in *Advances in Neural Information Processing Systems (NeurIPS)*, Long Beach, CA, USA, 2017, pp. 5998–6008.
- [53] Z. Liu, R. A. Yeh, X. Tang, *et al.*, “Video frame synthesis using deep voxel flow,” in *2017 IEEE International Conference on Computer Vision (ICCV)*, Venice, Italy, 2017, pp. 4473–4481.

#### APPENDIX

In the Appendix, we present the numerical analyses over the importance of delivering driving-critical information only. Taking the example of DSRC-based transmission systems [13], transmission latency ( $\tau_{ji}^{\text{tx}}$ ) represents the dominant temporal constraint, primarily caused by channel contention. Consider a typical traffic scenario involving up to 10 communicating agents (vehicles and RSUs). Assuming an ideal bandwidth ( $B$ ) of 20 MHz, where agent  $i$  seeks information from agent  $j$  located 50 meters away, and using the parameters specified in Table IV, transmission efficiency is impacted by packet loss, which is assumed to reach an upper bound of 5%, as shown in [10]. To model realistic conditions, where agent  $i$  simultaneously transmits and receives, the effective bandwidth is halved, and  $b_{ji}$  is distributed equally among the communicating vehicles. The transmission of an unprocessed semantic feature  $\mathcal{F}_j^t \in \mathbb{R}^{H \times W}$ , with size  $(\mathcal{F}_j^t) = 27$  Mb, is considered. Using the previous SOTA method [17], supported by empirical findings [63] and our results (Fig 9), the feature  $\mathcal{F}_j^t$  can be compressed to size  $(\widehat{\mathcal{F}}_j^{tr}) = 1$ Mb, yielding an average compression rate of 3.7%. As a result, based on Eq. (7), the transmission latency ( $\tau_{ji}^{\text{tx}}$ ) for agent  $j$ , located 50 meters from agent  $i$ , is approximately 67.6 ms, exceeding one SCHI. This necessitates deferring the transmission to the subsequent communication cycle, introducing an additional SI and culminating in a total transmission latency of 200 ms.

- [54] M. Jaderberg, K. Simonyan, A. Zisserman, *et al.*, “Spatial transformer networks,” in *Advances in Neural Information Processing Systems*, vol. 28, Montreal, Canada, 2015. [Online]. Available: [https://proceedings.neurips.cc/paper\\_files/paper/2015/file/33ceb07bf4eeb3da587e268d663aba1a-Paper.pdf](https://proceedings.neurips.cc/paper_files/paper/2015/file/33ceb07bf4eeb3da587e268d663aba1a-Paper.pdf)
- [55] E. Jang, S. Gu, and B. Poole, “Categorical reparameterization with gumbel-softmax,” in *International Conference on Learning Representations*, Virtual, 2022.
- [56] Y. Bengio, N. Léonard, and A. Courville, “Estimating or propagating gradients through stochastic neurons for conditional computation,” *arXiv e-prints*, pp. arXiv-1308, 2013.
- [57] K. Simonyan and A. Zisserman, “Very deep convolutional networks for large-scale image recognition,” in *3rd International Conference on Learning Representations (ICLR)*. San Diego, CA, USA: Computational and Biological Learning Society, 2015.
- [58] B. Jaeger, K. Chitta, and A. Geiger, “Hidden biases of end-to-end driving models,” in *2023 IEEE/CVF International Conference on Computer Vision (ICCV)*, Paris Convention Center, 2023.
- [59] X. Zhou, D. Wang, and P. Krähenbühl, “Objects as points,” *arXiv preprint arXiv:1904.07850*, 2019.
- [60] Y. Hu, S. Chen, Y. Zhang, *et al.*, “Collaborative motion prediction via neural motion message passing,” in *2020 IEEE/CVF Conference on Computer Vision and Pattern Recognition (CVPR)*, Seattle, WA, USA, 2020, pp. 6318–6327.
- [61] ASAM, “Asam opendrive standard,” <https://www.asam.net/standards/detail/opendrive/>.
- [62] R. Xu, H. Xiang, X. Xia, *et al.*, “Opv2v: An open benchmark dataset and fusion pipeline for perception with vehicle-to-vehicle communication,” in *2022 International Conference on Robotics and Automation (ICRA)*, Philadelphia, PA, USA, 2022, pp. 2583–2589.
- [63] R. Xu, H. Xiang, Z. Tu, *et al.*, “V2X-vit: Vehicle-to-everything cooperative perception with vision transformer,” in *Proceedings of the European Conference on Computer Vision (ECCV)*, Tel Aviv, Israel, 2022.

In other words, limited bandwidth or the substantial size of semantic features may prevent kinematic data transmission within a single CCHI, resulting in  $\tau_{ji}^{\text{tx}} \geq 50$  ms. Meanwhile, centralized methods driven by selection mechanisms [13] may fail to seize communication opportunities, resulting in suboptimal performance.